

Reversible manipulation of lattice defects in single-crystal SnO₂ microrod by applying mechanical stress and voltage

Cite as: J. Appl. Phys. **125**, 082512 (2019); <https://doi.org/10.1063/1.5053837>

Submitted: 27 August 2018 . Accepted: 08 October 2018 . Published Online: 06 December 2018

Makoto Sakurai, Kewei Liu, and Masakazu Aono



View Online



Export Citation



CrossMark

ARTICLES YOU MAY BE INTERESTED IN

[Real-time monitoring of stress evolution during thin film growth by in situ substrate curvature measurement](#)

Journal of Applied Physics **125**, 082513 (2019); <https://doi.org/10.1063/1.5054092>

[Strain engineering in functional 2-dimensional materials](#)

Journal of Applied Physics **125**, 082402 (2019); <https://doi.org/10.1063/1.5053795>

[Thermoelectric transport in torsional strained Weyl semimetals](#)

Journal of Applied Physics **125**, 082507 (2019); <https://doi.org/10.1063/1.5051966>

Lock-in Amplifiers up to 600 MHz

starting at

\$6,210



Zurich
Instruments

Watch the Video



Reversible manipulation of lattice defects in single-crystal SnO₂ microrod by applying mechanical stress and voltage

Cite as: J. Appl. Phys. **125**, 082512 (2019); doi: [10.1063/1.5053837](https://doi.org/10.1063/1.5053837)

Submitted: 27 August 2018 · Accepted: 8 October 2018 ·

Published Online: 6 December 2018



Makoto Sakurai,^{1,a)} Kewei Liu,^{1,2} and Masakazu Aono¹

AFFILIATIONS

¹WPI-Center for Material Nanoarchitectonics (MANA), National Institute for Materials Science (NIMS), 1-1 Namiki, Tsukuba 305-0044, Japan

²State Key Laboratory of Luminescence and Applications, Changchun Institute of Optics Fine Mechanics and Physics (CIOMP), Chinese Academy of Sciences (CAS), Changchun 130033, People's Republic of China

^{a)}E-mail: sakurai.makoto@nims.go.jp

ABSTRACT

We report a reversible transition between semiconducting and insulating states in a single-crystal SnO₂ microrod device through creation and healing of lattice defects by applying mechanical stress and voltage. The process of creating lattice defects by using mechanical stress is investigated using transmission electron microscope and photoluminescence observations. The results reveal the presence of slip planes and non-volatile lattice defects. The healing process is analyzed through the dynamic response of the current to the pulse voltage applied to the ends of the microrod. It is found that there are fast and slow healing processes. The fast process is due to field-induced reduction of the trapping potential barrier, and the slow one is due to Joule heating. The reversible and nonlinear nature of the defect manipulation will open new avenues of innovation different from those of conventional technology, especially for the mechanical design of touch interfaces.

Published under license by AIP Publishing. <https://doi.org/10.1063/1.5053837>

I. INTRODUCTION

Metal oxides' (ZnO, In₂O₃, SnO₂, Ga₂O₃, and TiO₂) nano/microwires have been studied for their novel electronic, optical, and chemical characteristics that have uses in electronics, optoelectronics, and chemical sensing, respectively.¹⁻¹² Their miniaturized devices have enhanced functionality and sensitivity of their intrinsic materials because of their large surface area to volume ratio.^{6,7} For further functionalization, metal nanoparticle deposition^{8,9} and core-shell formation^{6,7,10-12} have been used for oxide nano/microwires. Their properties can be modulated by external stimuli such as applied gate voltage, light irradiation, adsorbed molecules, or applied stress. Mechanical stress, in particular, changes the physical properties through the creation of strain and defects in oxide materials. ZnO nano/microwires have been studied by using mechanical stress for electro-mechanical applications, because their piezoelectric property enables mechanical energy to be converted

into electric energy.¹³⁻¹⁵ On the other hand, SnO₂ crystals do not have a piezoelectric property, because the rutile structure of the SnO₂ crystal has inverse symmetry. However, this rutile structure enables one to examine changes in the material's physical properties induced by lattice defects in bent nano/microwires without having to consider the surface charge caused by the piezo-electric effect. For this reason, we can investigate the effect of the defects directly. Recently, we have developed a technique for dynamic manipulation of lattice defects in a single-crystal SnO₂ microrod by the application of voltage and mechanical stress and achieved reversible semiconductor-insulator transitions at 300 K.^{16,17} The manipulation technique was applied to UV photodetectors of single-crystal SnO₂ microrods, and it solved the persistent photocurrent (PPC) problem in wide-bandgap semiconductors.¹⁸

Here, we review our studies on changes to structural and electronic properties due to mechanical-stress-induced

lattice defects. We report on electrical healing of defects in a single-crystal SnO_2 microrod device examined through dynamic measurements of the current in response to an applied pulse voltage and analyze the healing mechanism.

II. CREATION OF LATTICE DEFECTS BY MECHANICAL STRESS

A single-crystal SnO_2 microrod device exhibits a reversible semiconductor-insulator transition as a result of creation and healing of lattice defects under the application of mechanical stress and voltage at $T=300\text{ K}$ (Fig. 1).^{16,17} In this study, the microrods were grown by thermal evaporation in an electric furnace. The as-grown SnO_2 microrods had a square cross section with $1\text{--}2\ \mu\text{m}$ on a side. The microrods were n -type semiconductors with resistivities of $\sim 10\ \Omega\ \text{cm}$ at $300\ \text{K}$. Each microrod was placed on a flexible polymer substrate, and the voltage was applied to the ends while mechanical stress was also applied. The strain was due to the bending of the flexible substrate, caused by applying mechanical stress from the back (see the inset of the left panel of Fig. 1). When the strain was less than 0.2% , the resistance changed slightly and reversibly, suggesting that the microrod was deformed elastically. A further increase in strain induced a large and irreversible change in the resistance. Here, the microrod was deformed plastically, and the carriers in it were trapped at defect sites created by the deformation. Finally, the increase in the resistance due to the strain exceeded the instrumental limitation ($\sim 2 \times 10^7\ \Omega\ \text{cm}$), namely, the state of a microrod device changed into an insulating one. Interestingly, as the strain was decreased, the insulating state of the device recovered to

the original semiconducting state under the application of an appreciable voltage between the electrodes.

The structural changes caused by the mechanical stress were investigated using a transmission electron microscope (TEM; JEM-2100F, JEOL).¹⁷ The sample was a bent single-crystal SnO_2 nanowire instead of a bent microrod, because it is difficult for electrons accelerated in a conventional TEM to pass through SnO_2 microrods with a cross section of $1\text{--}2\ \mu\text{m}$ on one side. SnO_2 nanowires were synthesized in vapor growth using gold nano-clusters as catalysts in an electric furnace.^{17,19} They had rutile structures and grew in the $[001]$ direction. A single-crystal SnO_2 nanowire with a square cross section of about $100\ \text{nm}$ on one side was on a TEM grid, and then it was bent mechanically using a combined system of a focused ion microscope (FIB) and a nanoscale manipulator (NB5000, Hitachi, Ltd.). The procedure was observed with a scanning electron microscope (SEM). The bending process using a metal needle and localized tungsten (W) deposition is schematically illustrated in Fig. 2(a), while an SEM image of a bent SnO_2 nanowire fixed to the thin supporting carbon layer on the TEM grid is shown in Fig. 2(b). Holes at both ends of the nanowire in the low-magnification TEM image [Fig. 2(c)] were formed by localized tungsten deposition to fix the nanowire on the supporting layer.

Figure 3(a) shows a TEM image of the bent SnO_2 nanowire on the TEM grid. About 3% strain was applied to the outside of the nanowire. The dark stripes, indicated by the arrows, suggest lattice deformation and thickness differences. These would have been caused by the internal strain, because such stripes did not appear in the TEM images of the as-grown straight SnO_2 nanowires. The stripes were about

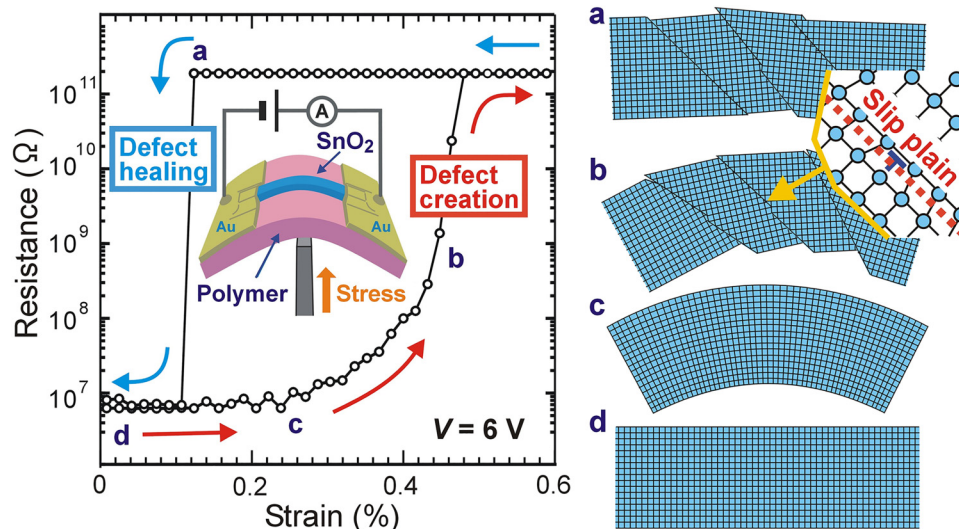


FIG. 1. Left panel: resistance of the SnO_2 microrod-based device as a function of strain at $V=6\text{ V}$ at 300 K . Inset schematically shows the microrod device on a flexible polyimide substrate under applied mechanical stress. Right panel: schematic illustrations of (a) disordered microrod, (b) plastically deformed microrod, (c) elastic bent microrod, and (d) original microrod, corresponding to the state marked in the left panel.

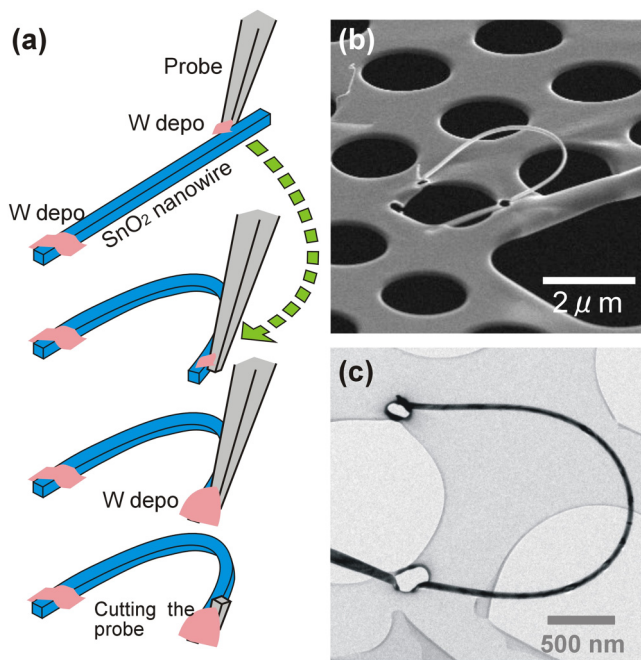


FIG. 2. (a) Schematic diagram showing fabrication of bent nanowires using a sharp metal probe and localized tungsten deposition in the FIB system. (b) SEM image and (c) TEM image of bent single-crystal SnO_2 nanowire on a thin carbon supporting layer of a TEM grid.

45° from the long wire direction. A magnified TEM image of the outer surface of the nanowire, where tensile stress was applied, reveals step-like structures [Fig. 3(b)]. The surface topography differed from that of the straight region, where the surface was almost flat. Split planes in rutile structures occur mainly along the $\langle 101 \rangle \{101\}$ plane and the $[001] \{110\}$ plane.^{20–22} The step-like structures and dark stripes in the TEM images could have been due to a slip along the $\langle 101 \rangle \{101\}$ plane caused by the applied tensile strain. Since dislocation was observed in the dark stripes of the bent wire,¹⁷ structural defects in the bent nanowire have been created by the slip and locally distributed around the slip plane, producing the dark stripes in Fig. 3(a). These results for the nanowire show that similar slip planes and structural defects could have been induced in single-crystal SnO_2 microrods bent by mechanical stress.

The electronic structure of a single-crystal SnO_2 microrod bent by mechanical stress was investigated using photoluminescence (PL) spectroscopy with an excitation source of 6.3 eV at 300 K [Fig. 4(a)]. There was no main peak due to direct electron-hole recombination across the bandgap ($E_g = 3.6$ eV) at 300 K.¹⁷ This is because carriers excited to the conduction bands quickly decay to levels arising from impurities and defects.²³ The energy band diagram of SnO_2 is drawn schematically in Fig. 4(b). To bend the microrod, a cantilever-type setup was used to remove background signals from the polymer substrate. One end of the microrod was fixed on the

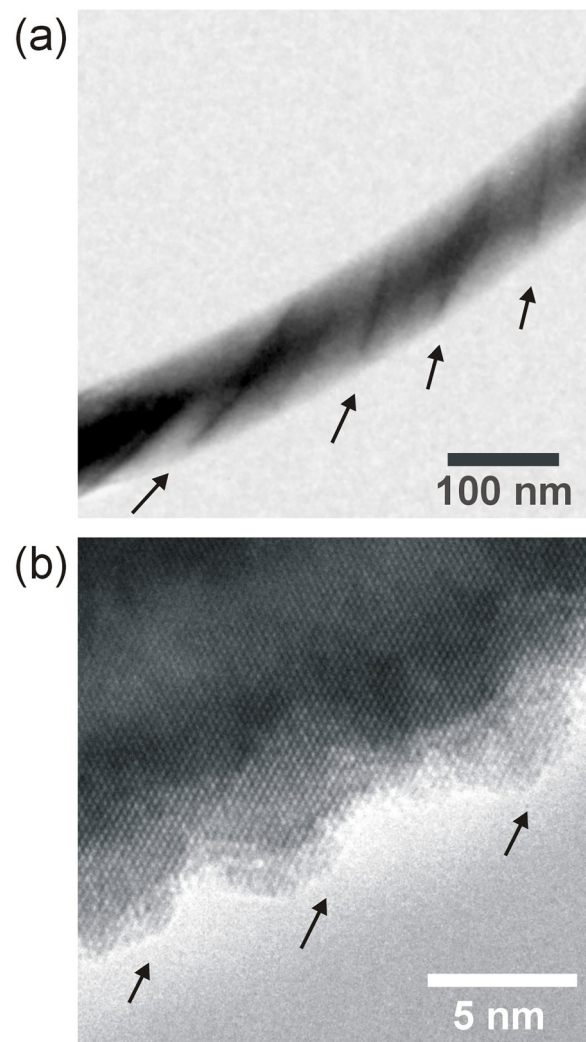


FIG. 3. (a) TEM image of bent single-crystal SnO_2 nanowire under 3% strain. Black stripes marked by arrows indicate the creation of slip planes in the rutile structure. (b) High-magnification TEM image of outer surface under tensile strain. Arrows indicate step-like surface structures.

stage, and the other free end was pushed by a mechanical positioner [Fig. 4(a)]. PL spectra were measured at 300 K for different strain states [Fig. 4(c)]. The broad visible emission was due to radiative electron-hole recombination between donor and acceptor levels, in which the acceptor levels were mainly due to oxygen vacancies.²⁴ As the strain ϵ of the microrod increased, the intensity became two to three times higher than that of the original straight microrod, suggesting that the number of lattice defects, e.g., oxygen vacancies, in the microrod increased as the strain increased. The intense visible emission remained even after the strain was released [bottom panel of Fig. 4(c)], suggesting that residual lattice

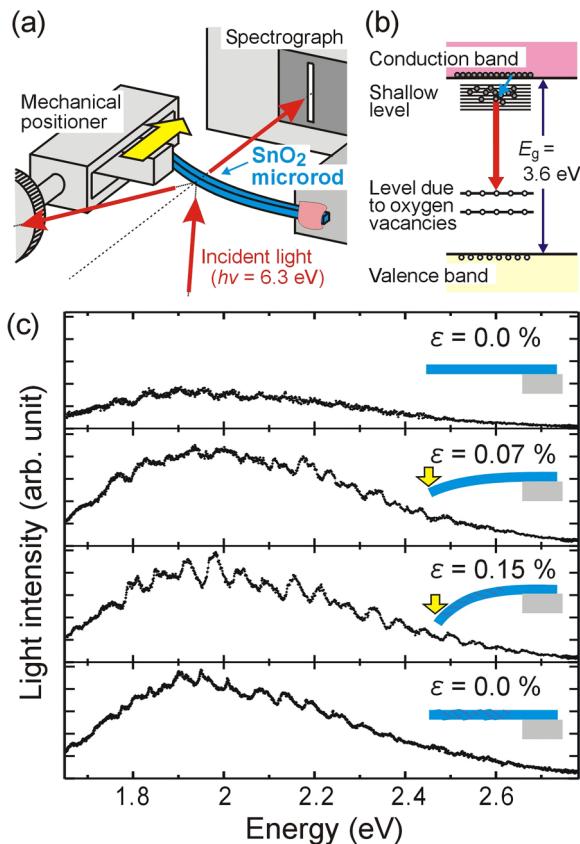


FIG. 4. (a) Experimental setup for PL measurement. (b) Schematic band diagram of SnO₂ with donor levels caused mainly by impurities and acceptor levels due to oxygen vacancies. (c) PL spectra of single SnO₂ microrod in different strain states at $T = 300$ K.

defects existed within the microrod ($\epsilon = 0$). This feature of defect creation as a function of strain is similar to the non-volatile response of resistance shown in Figs. 1 and 5(a). Therefore, we conclude that the strain in the single-crystal SnO₂ microrod induced slip planes in the rutile structure and that the slip produced many point defects such as oxygen vacancies near the planes. The deformed structure of the bent microrod shown with the resistance-strain curve in the left panel in Fig. 1 is schematically illustrated in the right panel.

The hysteresis behavior of the resistance-strain curve changes to a non-volatile one as the applied voltage decreases [Fig. 5(a)]. The threshold strain in going from the semiconducting state to the insulating state, at which the resistance of the bent microrod reaches the instrumental limitation of the resistance-strain curve measurement, is plotted against the voltage applied between the electrodes in Fig. 5(b) as closed circles. The threshold strain increased as the voltage increased, suggesting that electrical healing occurred at the same time as lattice defects were created by the strain. The threshold strain in going from the insulating state to the semiconducting

state, at which the resistance of the SnO₂ microrod in the insulating state departs from the instrumental limitation in the resistance-strain curve, is plotted in Fig. 5(b) as open circles. When the applied voltage was less than 4 V, the insulating state of the device retained after releasing the strain, suggesting a non-volatile insulating state.

III. DYNAMICS OF ELECTRIC HEALING OF LATTICE DEFECTS

A. Methods

The transient current of the healing process of the SnO₂ microrod device in the insulating state was measured for different combinations of mechanical stress and voltage pulses at 300 K in an ambient atmosphere [Fig. 6(a)]. A single-crystal SnO₂ microrod, whose sides were connected to Au electrodes, was placed on a sample stage. Mechanical strain was applied from the back of the substrate by using a linear positioner derived from a stepping motor (SPSG15-10, Sigma-Koki) with a precision of 1 μ m. The voltage pulse from a function generator (NF, WF1973) was applied to one electrode through a coaxial cable with a characteristic impedance of 50 Ω . The other electrode was connected to a preamplifier (Keithley, Current amplifier 428) through a coaxial cable to monitor the response of the current signal to the pulse voltage. The voltage was recorded (National Instrument, USB-6221) after current-voltage conversion with a gain of 10^7 V/A at the preamplifier. The experimental setting of electric instruments is similar to that of a scanning tunneling microscope.²⁵ Before each measurement, the microrod device was initialized by applying a large voltage of 10 V for ~ 30 s to heal the lattice defects. Then, the microrod was changed into the insulating state by bending the flexible substrate. The bending for the initialization was caused by moving the positioner vertically 800 μ m [Fig. 6(a)].

B. Dynamics of the electric healing process

The transition from the insulating state to the semiconducting state in the SnO₂ microrod device occurred by applying a pulse with a voltage of 7 V and a width of 1 ms [Fig. 6(b)]. The response curve included several features characteristic of defect healing. When the pulse voltage was applied to the device, sharp current peaks appeared at the rising and falling edges of the pulse. This behavior corresponds to a charging current accumulated in the parasitic capacitance of the metal-insulator-metal structure formed by the microrod and the Au electrodes. After the applied pulse, the current increased sharply with a certain time delay. It subsequently increased gradually, suggesting that there were two healing processes.

The delay time τ , defined as the time difference between the rising edge of the pulse and the rising of the sharp current [Fig. 6(b)], depends on the applied voltage [inset of Fig. 7(a)]. This feature indicates that the applied voltage affects the healing. Since the logarithm of τ is proportional to the voltage [Fig. 7(a)], the fast healing in the initial stage

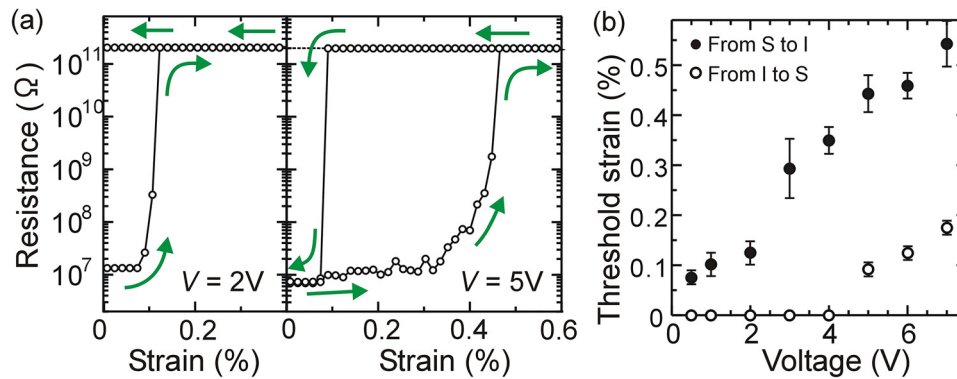


FIG. 5. (a) Resistance of the SnO_2 microrod device as a function of strain at $V = 2$ and 5 V at 300 K . (b) Threshold strain in transitions from semiconducting state to insulating state (closed circles) and from insulating state to semiconducting state (open circles) against voltage applied between the electrodes.

involves a voltage-induced reduction of the potential barrier E_A . Based on the Arrhenius law, the delay time τ can be described as

$$\tau = \tau_0 \exp[(E_A - qV)/k_B T]. \quad (1)$$

Here, τ_0 is a pre-exponential constant and qV is the barrier reduction effect caused by the applied voltage V . Since Eq. (1) is similar to the formula describing the Poole-Frenkel effect²⁶ and the electric field-induced barrier lowering for ion-migration,²⁷ we conclude that the fast healing at the initial stage is mainly due to the electric-field-induced reduction of the potential barrier for carriers and ionized atoms trapped at defect sites.

The transition from the insulating state to the semiconducting state in the SnO_2 microrod device depends on the pulse width of the applied voltage. Figure 7(b) shows the

relationship between the transition probability from the insulating state to the semiconducting state and the pulse width at three different applied voltages, suggesting that a small voltage applied to the device requires a long pulse width to complete the defect healing. Here, defect healing, such as a local rearrangement and migration of defects, needs thermal energy^{28–30} supplied by the electric power which is proportional to the applied voltage and time. The gradual increase in current after the sharp rise in Fig. 6(b) can be explained by slow healing through the Joule heating.

There are fast and slow healing processes in the SnO_2 microrod device in the insulating state. In order to understand the healing process, the electrical response of the device at 5.5 and 9 V was measured over a long time scale. For $V = 5.5\text{ V}$ [Fig. 8(a)], a sharp increase in current, $\sim 0.15\text{ }\mu\text{A}$, was observed after a time delay. About 4.5 ms after the onset of the pulse voltage, another sharp increase, $\sim 0.2\text{ }\mu\text{A}$, occurred.

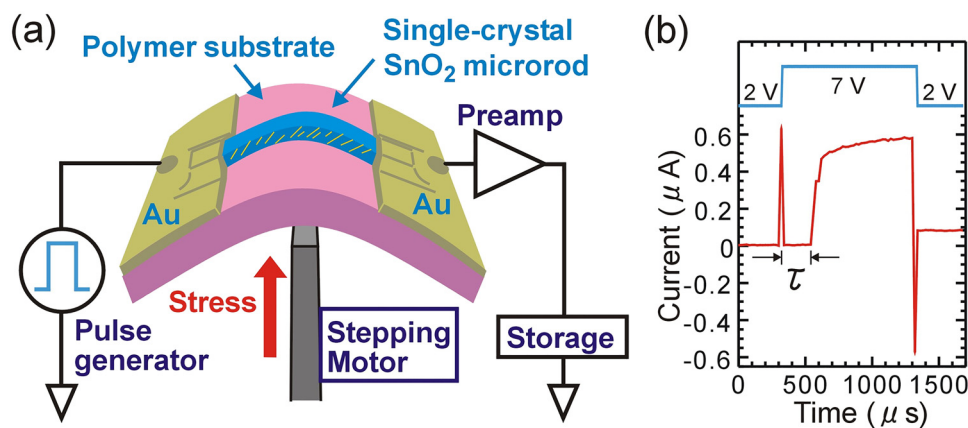


FIG. 6. (a) Schematic illustration of dynamic measurement of SnO_2 microrod devices under the application of pulse voltage. The spacing between the Au electrodes is $120\text{ }\mu\text{m}$ for a single-crystal SnO_2 microrod with a square cross-section of $2\text{ }\mu\text{m}$ on one side. (b) Typical transient current of device in the insulating state in response to pulse voltage ($V = 7\text{ V}$ and pulse width of 1 ms).

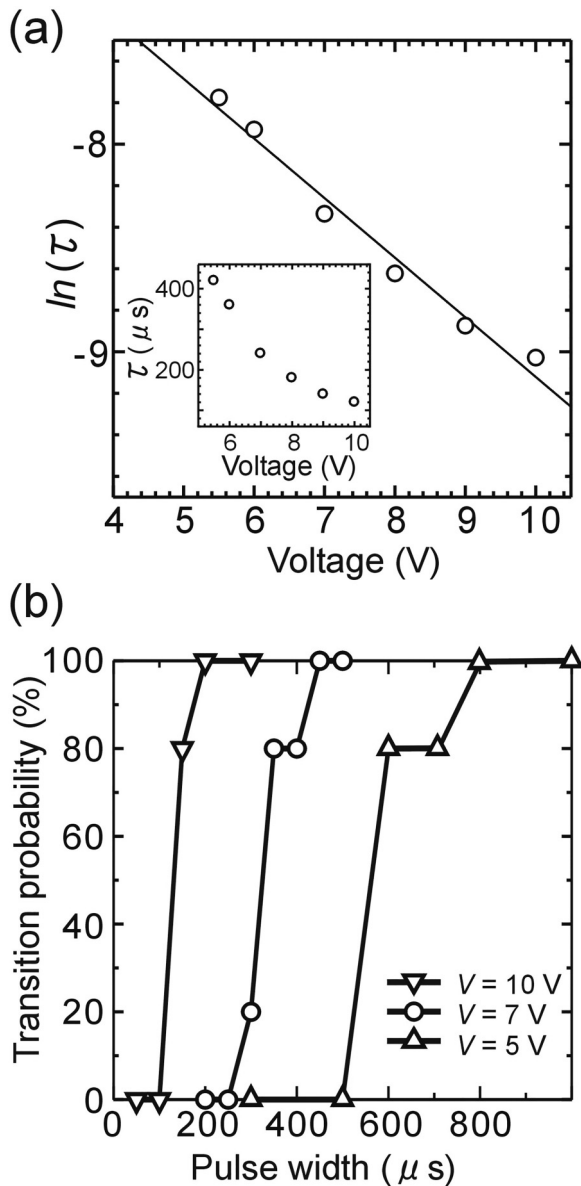


FIG. 7. (a) Inset: Time delay τ of response of SnO_2 microrod devices in the insulating state to each pulse voltage at $T=300$ K. The logarithm of τ has a linear relation to the applied voltage. (b) Transition probability from insulating state to semiconducting state in the microrod device as a function of pulse width for $V=5$, 7 , and 10 V at $T=300$ K.

For $V=9$ V [Fig. 8(b)], on the other hand, the current increased gradually after the sharp increase in the initial stage. The application of 5–6 V is not enough to release the trapped carriers and ionized atoms in the initial fast healing. Subsequent slow healing is required for their release.

The response of a SnO_2 microrod device in the insulating state to short voltage pulses was examined in order to

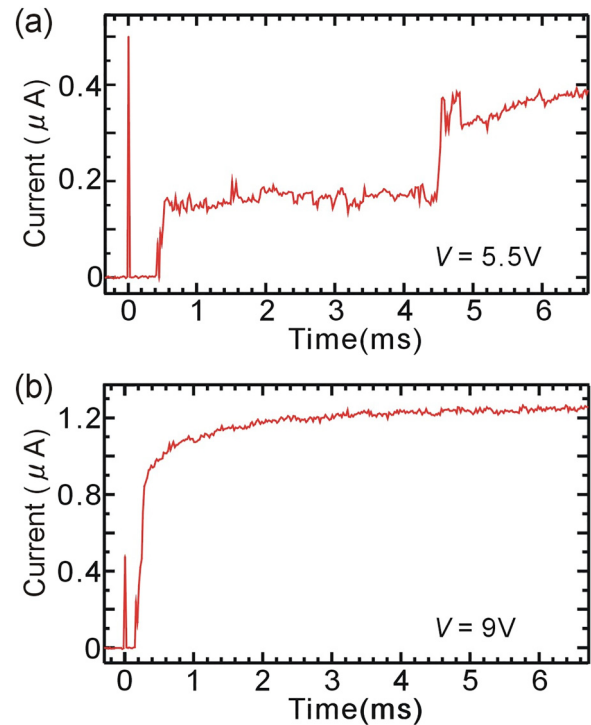


FIG. 8. Time-dependent response of the SnO_2 microrod device in the insulating state to the applied voltage of (a) 5.5 V and (b) 9 V at $T=300$ K.

understand the mechanism involved in the fast healing. Figure 9 shows the dynamic response of the device in the insulating state to a series of $220 \mu\text{s}$ and $400 \mu\text{s}$ pulses of $V=7$ V. The sharp changes in current at the rising and falling edges of the voltage pulse are due to charge accumulation. In the case of the $220 \mu\text{s}$ pulse [Fig. 9(a)], rising current was observed at the 7th pulse. Note that the delay of $\sim 100 \mu\text{s}$ at the 7th pulse is shorter than the standard delay time ($240 \mu\text{s}$) for a pulse voltage of 7 V [inset of Fig. 7(a)]. This result indicates that the insulating state of the microrod just before the 7th pulse is different from that at the first pulse and that the series of short pulses induce irreversible healing in the microrod, which the present instruments could not detect. The responses to the 8–10th pulses occurred without a time delay, suggesting that the incomplete small current path formed at the 7th pulse enables current to flow without a time delay and that the large current fluctuation during the pulse is due to simultaneous fast and slow healing. In the case of the $400 \mu\text{s}$ pulse [Fig. 9(b)], the current returned to the undetectable level just after the first pulse voltage fell. A subsequent gradual increase in current was observed during the OFF-period after the first pulse, where a voltage of 2 V was applied to monitor the state. The gradual increase without a time delay of the response to the 2nd and 3rd pulses suggests that the transition from the insulating state to the semiconducting state was completed during the OFF-period just after

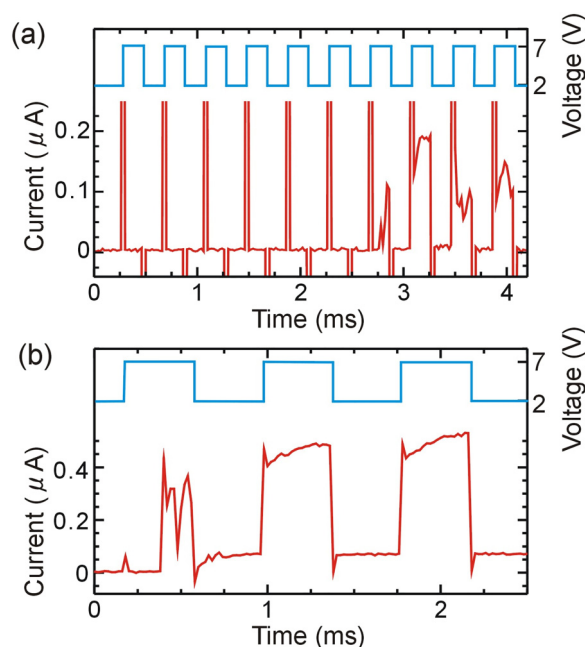


FIG. 9. Dynamic process of the device in the insulating state set by a series of (a) 220 μs and (b) 400 μs pulses of 7 V at $T = 300$ K.

the first pulse. This feature appearing in the response to a series of short pulses offers novel information about the progress of fast and slow healing.

IV. CONCLUSION

Our investigation of lattice defects created in the rutile structures using several defect manipulation techniques revealed that the reversibility of the lattice defects is due to the appearance of slip planes and lattice defects near the plane. There are two healing processes. One is a fast process, where carriers and ionized atoms trapped at defect sites are released when the trapped potential barrier is reduced by applying a voltage. The other is a slow process, where the local Joule heating induces a rearrangement of the atoms and defects, leading to gradual enlargement of the current path in the microrods. Our defect manipulation technique enabled us to find that the response of the lattice defects to the voltage and stress includes complex and nonlinear processes: competitive healing and creation of defects with different reaction speeds depending on the strain and applied voltage. This demonstration of using the defect manipulation technique to control such a complex system may pave the way for the development of new platforms for intelligent sensing and data processing different from those of conventional technology.

ACKNOWLEDGMENTS

The work was supported in part by the World Premier International Research Center (WPI) Initiative on Materials Nanoarchitectonics, MEXT, Japan, and in part by JSPS KAKENHI (No. K53640). We thank Dr. S. Shimomura and Dr. K. Miyazawa of NIMS for the operation of the FIB, Dr. K. Kurashima and Dr. I. Yamada of NIMS for the TEM measurements, and Dr. K. Watanabe of NIMS for measurement of the PL spectra.

REFERENCES

- Y. Xia, P. Yang, Y. Sun, Y. Wu, B. Mayers, B. Gates, Y. Yin, F. Kim, and H. Yan, *Adv. Mater.* **15**(5), 353 (2003).
- Ü. Özgür, Y. I. Alivov, C. Liu, A. Teke, M. A. Reshchikov, S. Doğan, V. Avrutin, S.-J. Cho, and H. Morkoç, *J. Appl. Phys.* **98**, 041301 (2005).
- W. Liu and C. M. Lieber, *J. Phys. D Appl. Phys.* **39**, R387 (2006).
- H. J. Fan, P. Werner, and M. Zacharias, *Small* **2**(6), 700 (2006).
- G. Shen, P. C. Chen, K. Ryu, and C. Zhou, *J. Mater. Chem.* **19**, 828 (2009).
- K. W. Liu, M. Sakurai, and M. Aono, *J. Mater. Chem.* **22**, 12882 (2012).
- K. W. Liu, M. Sakurai, and M. Aono, *Small* **8**(23), 3599 (2012).
- R. K. Joshi, Q. Hu, F. Am, N. Joshi, and A. Kumar, *J. Phys. Chem. C* **113**(36), 16199 (2009).
- K. W. Liu, M. Sakurai, M. Liao, and M. Aono, *J. Phys. Chem. C* **114**(46), 19835 (2010).
- X. Xue, L. Xing, Y. Chen, S. Shi, Y. Wang, and T. Wang, *J. Phys. Chem. C* **112**(32), 12157 (2008).
- L. E. Greene, M. Law, B. D. Yuhas, and P. D. Yang, *J. Phys. Chem. C* **111**(50), 18451 (2007).
- S. Park, A. An, Y. Mun, and C. Lee, *ACS Appl. Mater. Inter.* **5**(10), 4285 (2013).
- Z. L. Wang and J. Song, *Science* **312**, 242 (2006).
- Y. Gao and Z. L. Wang, *NANO Lett.* **7**(8), 2499 (2007).
- Y. Lin, P. Deng, Y. Nie, Y. Hu, L. Xing, Y. Zhang, and X. Xue, *Nanoscale* **6**, 4604 (2014).
- K. W. Liu, M. Sakurai, and M. Aono, *ACS Nano* **6**(8), 7209 (2012).
- M. Sakurai, K. W. Liu, and M. Aono, *Appl. Phys. Express* **7**, 031101 (2014).
- K. W. Liu, M. Sakurai, M. Aono, and D. Shen, *Adv. Funct. Mater.* **25**, 3157 (2015).
- M. Sakurai, Y. G. Wang, T. Uemura, and M. Aono, *Nanotechnology* **20**, 155203 (2009).
- M. G. Blanchin and G. Smallman, *Phys. Status Solidi* **A29**, 491 (1975).
- K. H. G. Ashbee and R. E. Smallman, *Proc. R. Soc. Lond.* **A274**, 195 (1963).
- K. H. G. Ashbee and R. E. Smallman, *J. Am. Ceram. Soc.* **46**, 211 (1963).
- A. Othonos, M. Zervos, and D. Tsokkou, *Nano. Res. Lett* **4**, 828 (2009).
- A. Kar, S. Kundu, and A. Patra, *J. Phys. Chem.* **C115**, 118 (2011).
- C. J. Chen, *Introduction to Scanning Tunneling Microscopy* (Oxford University Press, New York, 1993), Chap. 11.
- T. E. Hartman, J. C. Blair, and R. Bauer, *J. Appl. Phys.* **37**, 2468 (1966).
- D. Ieimini, in *Nanoscale Applications for Information and Energy Systems*, edited by A. Korkin and D. J. Lockwood (Springer, New York, 2013), Chap. 6.
- R. D. Doherty, D. A. Hughes, F. J. Humphreys, J. J. Jonas, D. J. Jensen, M. E. Kassner, W. E. King, T. R. McNelley, H. J. McQueen, and A. D. Rollett, *Mater. Sci. Eng. A* **238**, 219 (1997).
- Y. Wu and P. Yang, *Adv. Mater.* **13**(7), 520 (2001).
- T. S. Sakhivel, D. L. Reid, U. M. Bhatta, G. Möbus, D. C. Sayle, and S. Seal, *Nanoscale* **7**, 5169 (2015).